Elaboration and characterization of new phosphate glasses based on natural phosphate and red clay: influence of the chemical composition on the chemical durability

Oumaima Jamal Eddine [1,*], Mehdi El Bouchti [2], Omar Cherkaoui [2], Hassan Hannache [1,3] and Said Gmouh [1]

[1] University Hassan II of Casablanca, Faculty of Sciences Ben M'Sik, Chemistry Department, LIMAT, Avenue Driss El Harti, Casablanca, Morocco

[2] Higher School of Textile and Clothing Industries, Laboratory REMTEX, km 8, Route d'El Jadida, BP 7731 – Oulfa, Casablanca, Morocco

[3] University Mohammed VI Polytechnic, Materials Science and Nanoengineering Department, Lot 660, Hay Moulay Rachid, Benguerir, Morocco

Abstract: New phosphate glass formulations based on Moroccan natural phosphate minerals alone or with Moroccan red clay additive (containing the P_2O_5-SiO_2-CaO-Al_2O_3-MgO-Fe_2O_3-K_2O-Na_2O-TiO_2 complex) have been successfully prepared by the quenching method. The chemical composition of each of the elaborated phosphate glasses was determined by X-ray fluorescence analysis (XRF). These investigated phosphate glasses have an excellent homogeneity as was verified by SEM. Their amorphous behavior was confirmed by XRD and DSC. The increase in density and glass transition temperature due to the addition of clay is believed to be related to the crosslinking of the phosphate chains. Structural investigation of these phosphate glasses was carried out using FTIR and Raman spectroscopies. The results obtained show that the composition of these glasses contains a mixture of ultraphosphate and polyphosphate structural units. The concentrations of this mixture depending on the initial composition of the glass components. A correlation between the chemical composition and the chemical durability of the investigated glasses was studied. The results showed that the dissolution rate of the glasses decreases by increasing the clay composition up to a point. This can be explained by assuming the formation of oxygen bridges and strong bonds within the various glasses.

Keywords: Natural phosphate; Red clay; Phosphate glasses; Chemical composition; Chemical durability.

1. Introduction

Phosphate glasses (PGs) currently compete with silica glasses because are characterized by their high UV transparency, low IR transparency, and high thermal expansion, as well as their electrical and optical characteristics. Owing to these properties, phosphate glasses offer a unique range of applications, such as glass-polymer composite materials [1], slow-release fertilization [2], nuclear waste immobilization matrices [3], conductive materials [4] amorphous semiconductors [5], optical waveguides [6], and solid-state laser [7].

Phosphate glasses are mainly composed of tetrahedral units PO_4^{3-}. The double bond (P=O) in these tetrahedra causes polarization of the other P-O bonds and increases the ionicity of the P-O-M bonds (with M = Fe, Zn, Al, B, Pb, Si, N...). This limits the rate of glass crosslinking by minimizing the network condensation and making the composition easily hydrolysable [8,9,10]. It is this major disadvantage of phosphate glasses, their poor chemical durability against corrosion agents, that has dramatically limited their development [8,11,12]. In order to solve this problem, it has been shown by others that the introduction of multivalent cations allows the formation of more covalent bonds and the reinforcement of glassy networks against hydrolysable attack through the formation of ionic crosslinking P-O-M bonds [2,8,10-17].

In recent years, complex phosphate glasses have attracted increasing interest. For example, Brauer and al. [14] studied a quaternary phosphate glass system P_2O_5–CaO–Na_2O–MgO–TiO_2 which reported that the addition of titanium oxide produced glasses that were more stable to dissolution. Khan et al. [13] have reported a quaternary phosphate glasses in the glassy system P_2O_5–CaO–Na_2O–MgO–Fe_2O_3 and

found that the addition of Fe_2O_3 makes the phosphate glasses of this system more durable which can be explained by the formation of Fe-O-P bonds which replaces that of P-O-P. Waclawska et al. [2] studied the influence of the addition of ZnO on the structure of multicomponent glasses system SiO_2-P_2O_5-K_2O-CaO-MgO-ZnO acting as a slow-release fertilizer, and found that the introduction of up to 15 mol% of ZnO substituting CaO and MgO into the structure of the studied glasses causes the depolymerisation of the silicate phosphate network. In addition, other works show that the rate of degradation decreases with increasing content of some elements such as Al, Mg, N, B, and Zr [3,9,12,17,18].

In this context, the objective of this work was on the one hand to develop new formulations of phosphate glasses based on inexpensive raw minerals, from which we used Moroccan natural phosphate and Moroccan red clay. On the other hand, we wished to increase the chemical durability of phosphate glasses, which strongly depends on their compositions, structures, etching solution, temperature and pH of the solution [13,14,17]. The phosphate glasses synthesized contain all the macroelements (P, Ca, Mg, and K) and microelements (Si, Al, Fe, Na, and Ti) would then be used to develop phosphate glass fibers acting as a slow-release fertilizer, with high chemical durability and high mechanical resistance.

2. Experimental

2.1. Raw materials

Natural raw materials used in this study were: Moroccan natural phosphate (NP) extracted from one of the mines of the Ouled Abdoun basins in Khouribga region, and Moroccan red clay (RC): extracted from Berrechid region, which belongs to the western Moroccan Meseta (red triassic clays). The mineralogy of the raw materials was determined by XRF, XRD, and FTIR.

2.2. Glass preparation

A series of multicomponent phosphate glasses (PGs) systems were prepared by mixing the natural phosphate (NP) and the red clay (RC) in crude forms separately (RC-x: x=0, 2, 5, 10, or 15 (in weight percentage of RC (wt%)). A reference glass without the addition of clay was also prepared (NP-glass or RC-0). These five glasses were prepared using the melt-quenching method. The mixture corresponding to the desired compositions was firstly heated at 600°C for 2h. Then the temperature was progressively raised from 600°C to 1100°C, depending on the glass composition and held constant for 1h in an electrically heated furnace. The molten liquid was quenched to room temperature under the air atmosphere in order to produce a vitreous network. Table 1 shows the photographs of the elaborate phosphate glasses.

Table 1. Photographs of the elaborate phosphate glasses.

Glass code	NP-glass	RC-2	RC-5	RC-10	RC-15
Glass sample					

2.3. X-Ray Fluorescence analysis

Chemical analysis of the raw materials and the annealed phosphate glasses (PGs) samples was carried out by X-Ray Fluorescence spectrometer (XRF).

2.4. SEM analysis

The SEM micrographs of the PGs were recorded using a ZEISS Supra 55VP scanning electron microscope operating under high vacuum at 3 kV and using a secondary electron detector (Everhart–Thornley detector). A sample of phosphate glass was dried and then deposited on the surface of an adhesive carbon film, and a 20 nm gold coating was sputtered on the surface to make them conductive.

2.5. X-ray diffraction analysis

The amorphous behaviour of the elaborated PGs was confirmed by the XRD analysis using a Siemens D501 diffractometer, equipped with a copper anticathode tube and a secondary monochromatic (Cu-Kα radiation λ_{Cu} = 1.5406 Å).

2.6. Thermal analysis

The glass transition temperatures (Tg) were determined by DSC on 20 to 30 mg of beautiful powder samples of phosphate glass using the TGA/DSC 1 (Mettler Toledo) with 10°C min^{-1} constant heating rate (accuracy ± 2°C) under argon flow. The apparatus cools under nitrogen.

2.7. Density and molar volume measurement

The densities of the PGs were measured at room temperature via Archimedes method according to BS 10119 [19], in which ethanol (from Sigma-Aldrich) was used as the working fluid using Eq. (1). The error of the density measurements was within ± 0.03 g.cm^{-3}. The molar volume was calculated

from the density of glass and the molar weight ($V = M/\rho_g$).

$$\rho_g = (m_a / (m_a - m_w)) \times \rho_e \qquad (1)$$

Where ρ_g is the density of glass sample, ρ_e is the density of ethanol, m_a is the mass of dry glass weighed in air, and m_w is the mass of glass immersed in ethanol.

2.8. FTIR spectroscopy

The FTIR absorption spectra of PGs were made using a Thermo Electron (Nicolet 5700-FTIR model) spectrometer equipped with diamond micro-ATR accessory and recorded in the range of 400-4000 cm^{-1}.

2.9. Raman spectroscopy

The Raman spectra of PGs were recorded at room temperature in the 200-3300 cm^{-1} range using a Thermo Fisher XRD 2 RAMAN spectrometer equipped with an internal He–Ne laser source (8 mW) under an excitation $\lambda = 633$ nm and a CCD detector (Thermo, USA).

2.10. Chemical durability

Each solid glass sample was first annealed at (Tg-20) °C for 8h to eliminate residual stresses, then cut and dry polished using standard SiC abrasive paper to a circular shape to avoid preferential corrosion. Then each piece of glass was washed with acetone and dried at 102°C for 30 minutes. The sample thus prepared was weighed and then placed in a flask containing the already prepared alternative solution (pH = 5; 7; and 8), then heated to a temperature of 30 ± 3°C under agitation for 6 days. The pH of each alternative solution was adjusted by a buffer solution whose composition is presented in Table 2. After filtration, each glass sample was rinsed with acetone

and dried at 102°C for 30 minutes. The final mass and dimensions of the glass piece were then measured.

Table 2. Composition of the buffer solution [20].

pH ± 0.1	Composition
5	Acetic acid + sodium acetate
7	Acetic acid + concentrated ammonia
8	Acetic acid + concentrated ammonia

The chemical durability of investigated phosphate glasses was evaluated in terms of dissolution rate (D_R) as weight loss per unit surface area per unit time (g.cm^{-2}.min^{-1}) according to Eq. (2):

$$D_R = \Delta m / (S \times t) \qquad (2)$$

Where Δm is the mass loss (g), S is the surface area (cm^2) of the glass, and t is the time (min) of immersion of the glass in the solution. The estimated error was calculated to be ± 2 g.cm^{-2}.min^{-1}.

3. Results and Discussion

3.1. Raw material characterization

The combination of the results of different analysis methods: XRF, XRD and FTIR allowed us to determine the chemical and mineralogical compositions of the minerals used in this study. Table 3 presents the standardized results of the XRF analysis of the raw materials (%wt). The results of the chemical analysis show that the NP contains significant percentages of CaO, P_2O_5, whereas the RC analysis showed a dominance of silica and relatively high concentrations of Al_2O_3, as well as a higher percentage of Fe_2O_3, K_2O, and MgO.

Table 3. Chemical analysis (wt%) of the raw materials.

	Oxides	P_2O_5	CaO	SiO_2	Al_2O_3	Fe_2O_3	MgO	K_2O	Na_2O	TiO_2	MnO	ZnO
Raw material, (wt%)	NP	34.97	58.88	3.67	0.44	0.26	0.70	0.08	0.92	0.03	0.01	0.03
	RC	0.16	3.74	60.50	17.71	7.36	3.99	5.10	0.55	0.76	0.11	--

The X-ray pattern obtained for the NP (Fig. 1a) shows the presence of the following phases: fluorapatite $Ca_5(PO_4)_3F$ as the primary phase, calcium carbonates $CaCO_3$ (calcite) and quartz SiO_2. The latter two are exogangue in nature, and the interference of these phases with fluorapatite is due to their endogangue nature. Jointly, they constitute the francolite. In addition, it should be noted that there are small peaks of minority phases and that there may also be amorphous phases.

The bands observed in the infrared spectrum of the NP (Fig. 1b) can be divided into different domains: those between 950 cm^{-1} and 1110 cm^{-1} are attributed to the symmetrical and asymmetrical elongation

vibrations of the PO_4 groups; those between 460 cm^{-1} and 602 cm^{-1} are attributed to the symmetrical deformation vibrations of the PO_4 groups; valence vibrations of calcite $CaCO_3$ groups are observed at 1426 cm^{-1} and 1454 cm^{-1}; the adsorption bands centred at 1812 cm^{-1}, 1637 cm^{-1}, 795 cm^{-1}, and 648 cm^{-1} are attributed to traces of the carbonyl compounds; in addition, the stretching vibration bands between 780 cm^{-1} and 800 cm^{-1} are assigned to the vibration of the silicate groups. The infrared spectrum of the Khouribga NP shows no characteristic absorption band of OH$^-$ hydroxyl ions at 3560 cm^{-1} and 630 cm^{-1}, confirming that this phosphate is a carbonate fluorapatite (francolite)
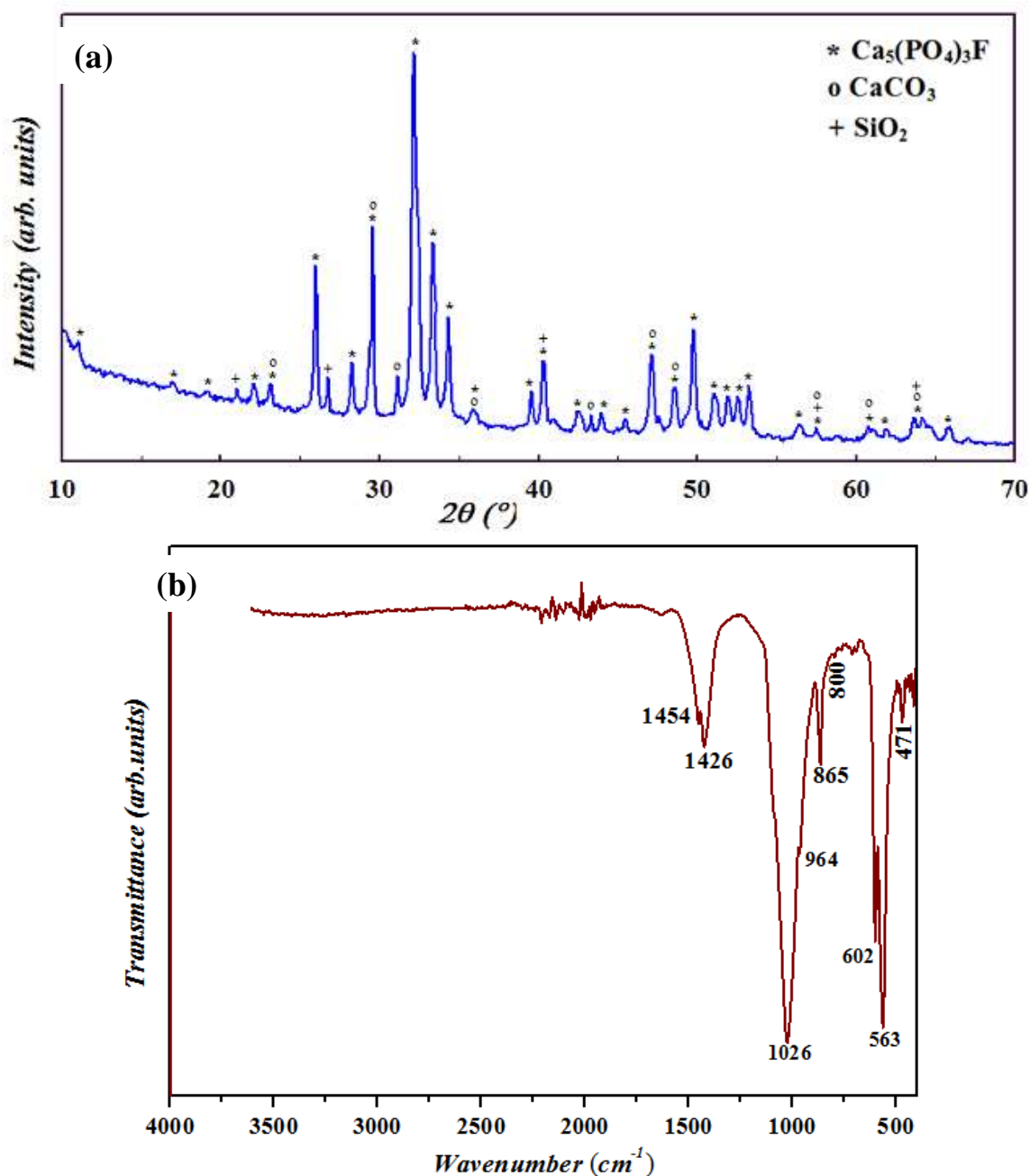
Figure 1. (a) X-ray diffractogram and (b) Infrared spectrum of natural phosphate from Khouribga.

The X-ray pattern of the red clay (Fig. 2a) shows a predominance of quartz (SiO_2) and kaolinite ($Al_2Si_2O_5(OH)_4$), as well as illite ($K_{0,75}Na_{0,01}Mg_{0,15}Fe_{0,04}Al_{2,59}Si_{3,27}O_{10}(OH)_2$) and muscovite $KAl_2(Al\ Si_3O_{10})(OH)_2$ which have very similar peaks. This does not allow easy distinction between the two phases [21]. The results showed also the presence of chlorite $(Mg, Fe, Al)_6[AlSi_3O_{10}](OH)_8$ and hematite Fe_2O_3, as well as calcite $CaCO_3$ and dolomite $MgCa(CO_3)_2$ as an impurities source. These results show that this natural clay is rich in clay minerals and poor in carbonates. Nonetheless, it was found within perfect agreement with the results of XRF, which shows high proportions of SiO_2 and Al_2O_3 and an expected presence of iron, potassium, magnesium, and calcium content. In addition, the $SiO_2/Al_2O_3=3.4$ ratio is a characteristic index of free quartz [22].

The infrared spectrum of the RC obtained is illustrated in Fig. 2b. The frequencies and their allocations are given in Table 4. Infrared spectroscopy was used to complete the analysis of the clay sample. The results are in agreement with those found from XRD. They confirm the presence of quartz and kaolinite as major phases and carbonate as a minor phase in the red clay studied.
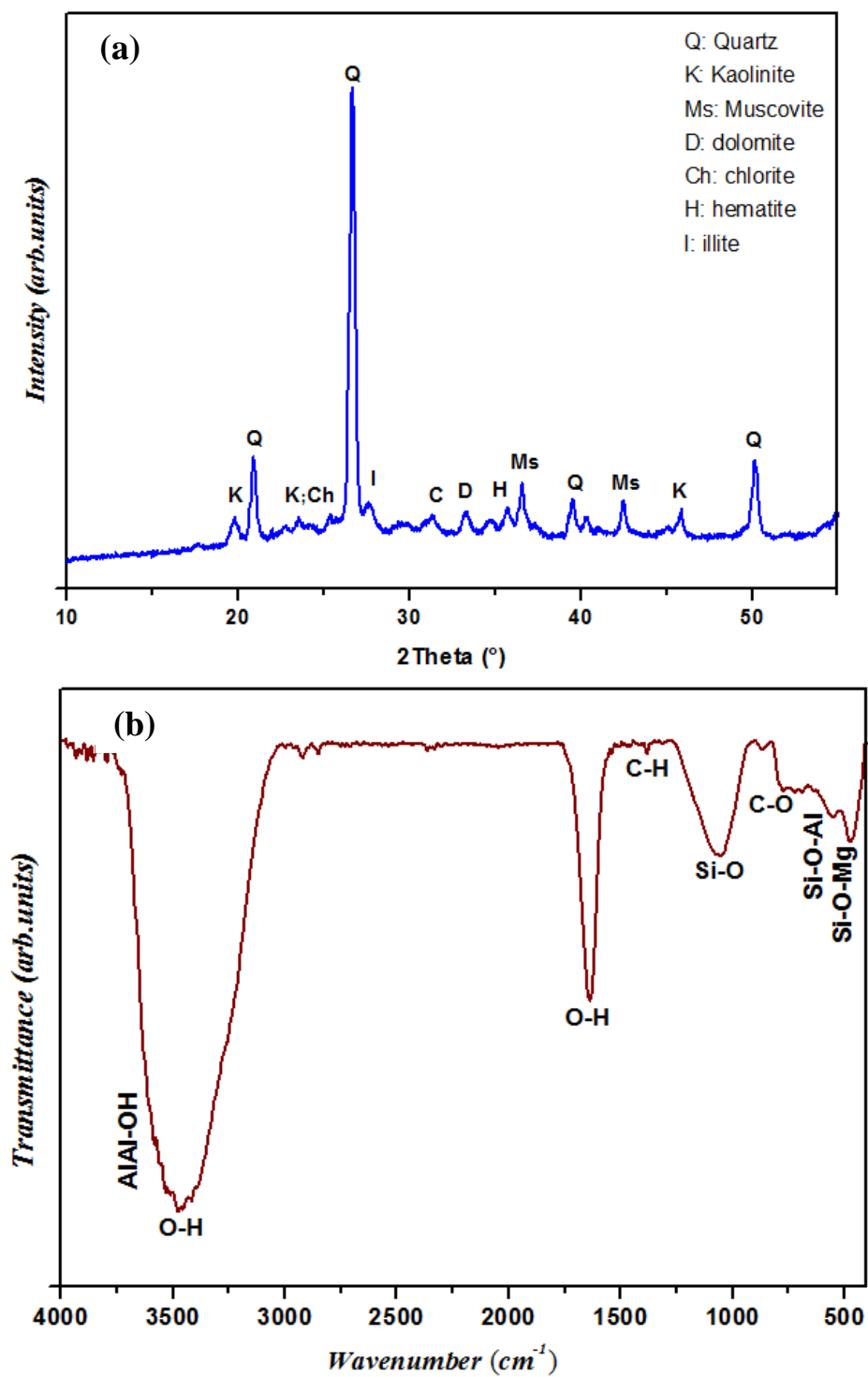
Figure 2. (a) X-ray diffractogram and (b) Infrared spectrum of the red clay from Berrechid.

Table 4. Frequencies (cm^{-1}) and allocations of infrared bands characteristic of the red clay from the Berrechid region.

Wavenumber (cm^{-1})	Attributions
3585	Between 3700 cm^{-1} and 3620 cm^{-1}: vibrations of the structural hydroxyl groups AlAl-OH characteristic of kaolinite
3477	Wideband around 3477 cm^{-1} indicating the presence of a hydroxyl group (O-H stretching vibrations)
1796	Between 1770 cm^{-1} and 1800cm^{-1}: Elongation vibration C=O
1634	Deformation vibration of free H_2O
1383	Between 1500 cm^{-1} and 1400 cm^{-1}: Symmetrical deformation vibration of the CH$_3$ groups around 1383 cm^{-1}
1058	Elongation vibration of the Si-O bond of kaolinite or quartz
870 and 722	Characteristic bands of C-O carbonates
778	Quartz
628	Vibrations characteristic of Si-O or Si-OH (deformation) and/or Al-O (elongation)
556	Deformation vibration of the Si-O-Al bond
474	Between 550 cm^{-1} and 400 cm^{-1}: deformation vibration of the Si-O-Mg bond that partially overlaps with the Si-O bending absorption, resulting in a single strong band located near 474 cm^{-1}

3.2. Glass Characterization

3.2.1. X-ray fluorescence analysis

The structure of the phosphate glasses is highly dependent on the oxygen/phosphate (O/P) ratio, which varies according to the oxide content in these glasses, as demonstrated by several previous studies [2,9,23-26]. The calculated values of O/P are summarized in Table 5. For the reference glass (NP-glass) containing 50 mol% of P_2O_5, the ratio was O/P= 2.73, and when 2% and 5% by weight of the red clay were added (RC-2 and RC-5), the ratio increased to O/P= 2.91 and 2.97 respectively, which characterizes

the ultraphosphate glasses (5/2< O/P <3) of a long phosphate chain with 3 oxygen bridges (Q^3). When 10% and 15% by weight of clay were added, the ratio increased to O/P= 3.08 and 3.13 respectively for RC-10 and RC-15 phosphate glasses. This is the case for polyphosphate glasses, which are made up of infinite chains of PO$_4$ tetrahedra (Q^2 chains ending in Q^1 units). Similar results were obtained by Ahmed et al. [11] who found that Q^3 species were present in glasses containing more than 50 mol% of P_2O_5 and Q^1 species were present in glasses containing less than 50 mol% P_2O_5.

Table 5. Chemical compositions of the PGs in weight percent (wt%) and molar percent (mol%).

Glass code	Chemical composition																				O/P
	P_2O_5		CaO		SiO_2		Al_2O_3		Fe_2O_3		MgO		K_2O		Na_2O		TiO_2		ZnO	
	wt%	mole	wt%	mol%	wt%	mol%	wt%	mol%	wt%	mol%	wt%	mol%	wt%	mol%	wt%	mol%	wt%	mol%	wt%	
NP-glass	70.81	50	25.06	45	2.46	4.09	0.61	0.60	0.14	0.09	0.38	0.94	0.08	0.09	0.41	0.66	0.03	0.04	0.02	2.73
RC-2	66.60	47	16.11	29	7.25	12.07	4.74	4.65	2.32	1.45	1.20	2.98	1.41	1.50	0.24	0.39	0.13	0.16	0.00	2.91
RC-5	65.05	46	14.10	25	9.34	15.55	5.25	5.15	2.94	1.84	1.35	3.35	1.59	1.69	0.23	0.37	0.15	0.19	0.00	2.97
RC-10	60.00	42	13.87	25	13.92	23.17	4.26	4.18	3.66	2.29	1.49	3.70	2.33	2.47	0.30	0.48	0.17	0.21	0.00	3.08
RC-15	58.38	41	13.86	25	14.11	23.49	3.94	3.86	4.68	2.93	1.46	3.62	3.02	3.21	0.38	0.61	0.17	0.27	0.00	3.13

3.2.2. SEM analysis

All samples of the prepared phosphate glasses appear transparent and homogeneous under daylight (Table 1). The following figure (Fig. 3) shows two examples of SEM micrographs of NP-glass phosphate glass (Fig. 3a) and RC-15 phosphate glass fractions (Fig. 3b). As expected, the surface is smooth that there are no cracks were visible on the surface at 500 times magnification.
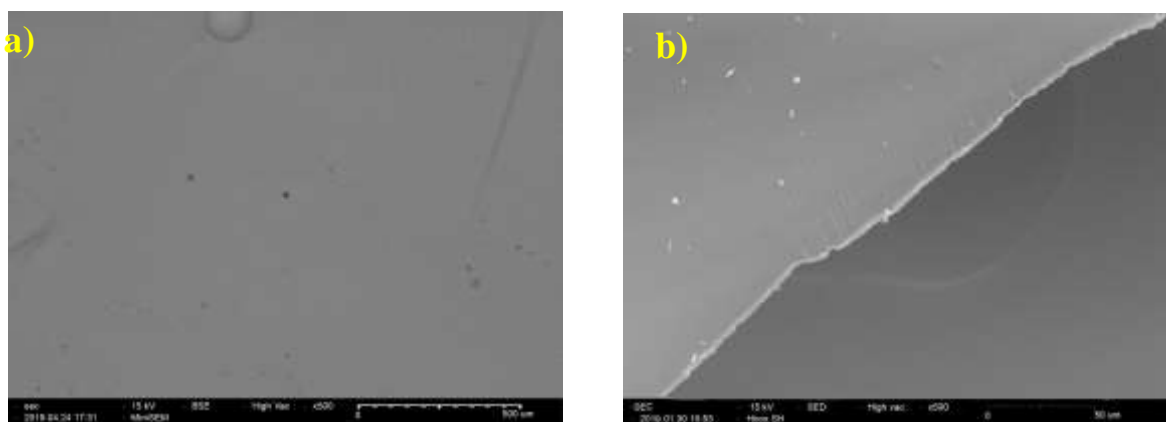

Figure 3. SEM micrographs (x 500) of two PGs: (a) reference glass (NP-glass), and (b) glass contains 15% of red clay (RC-15).

3.2.3. X-ray diffraction analysis

XRD patterns of all compositions of elaborated PGs are shown in Fig. 4. All spectra of glasses showed a lack of sharp peaks between 10° and 70° (2θ), which characterizes long-range disorder in the vitreous network.
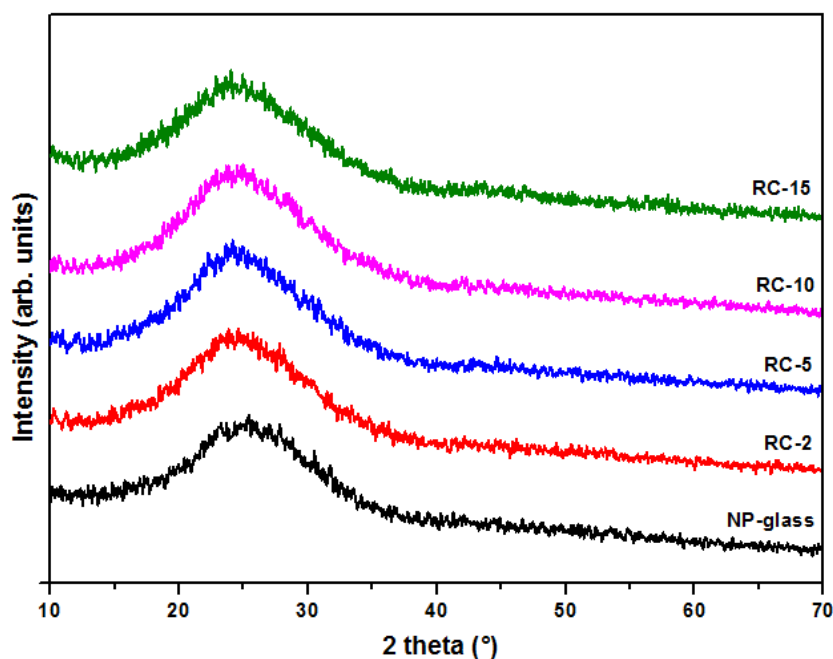

Figure 4. XRD spectra of elaborated phosphate glasses.

3.2.4. Density, molar volume, and thermal analysis

The density of glass is an important factor in determining the degree of change of the structure within the glass as the composition of the glass changes due to the addition of modifying oxides. The values of the calculated density and molar volume measurements of phosphate glass samples studied here are given in Table 6, while the variation of these two factors concerning the amount of clay added is presented in Fig. 5.

The results showed that the density of glasses gradually increases with the clay content in the glass, which increases from $\rho_g= 2.6359$ g.cm^{-3} for reference glass to $\rho_g= 2.9542$ g.cm^{-3} for RC-15. Conversely, the molar volume decreases monotonously with the introduction of clay. It varies from Vm= 44.54 for NP-glass to Vm= 38.73 for RC-15.
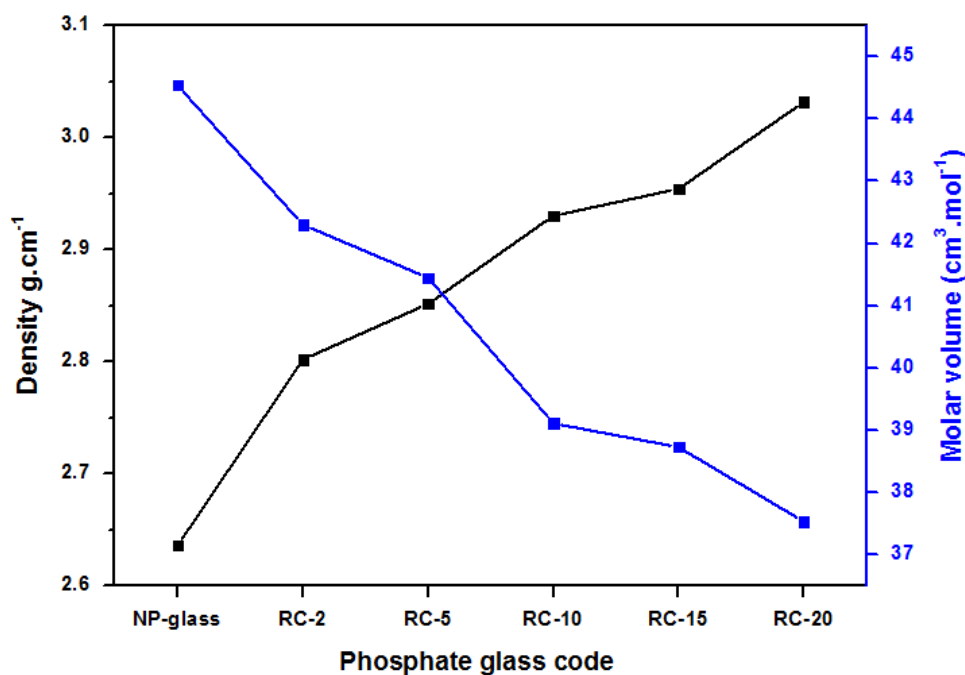
Figure 5. Composition dependence of density and molar volume of PGs containing red clay.

Fig. 6 shows DSC curves of NP-glass, RC-5, and RC-15 phosphate glasses. The values of the glass transition temperature (Tg) are given in Table 6. The results show that the Tg values increase with the clay content in the phosphate glass. It varies from 392°C for NP-glass to 491°C for RC-15. Thus, this increase in Tg could be correlated to several factors such as the modification of the bond strength and the crosslinking of the glassy network with the increase in atomic packing due to the incorporation of M ions belonging to the clays with the formation of the P-O-M bonds (with M= Si, Fe, Al, and Mg), which become covalent with a higher rate of clay oxides, which allows the reinforcement of the glassy networks [18,20,27,28]. This result is well correlated with the evolution of density and molar volume measurements that suggest the compactness of the glass structure [27].
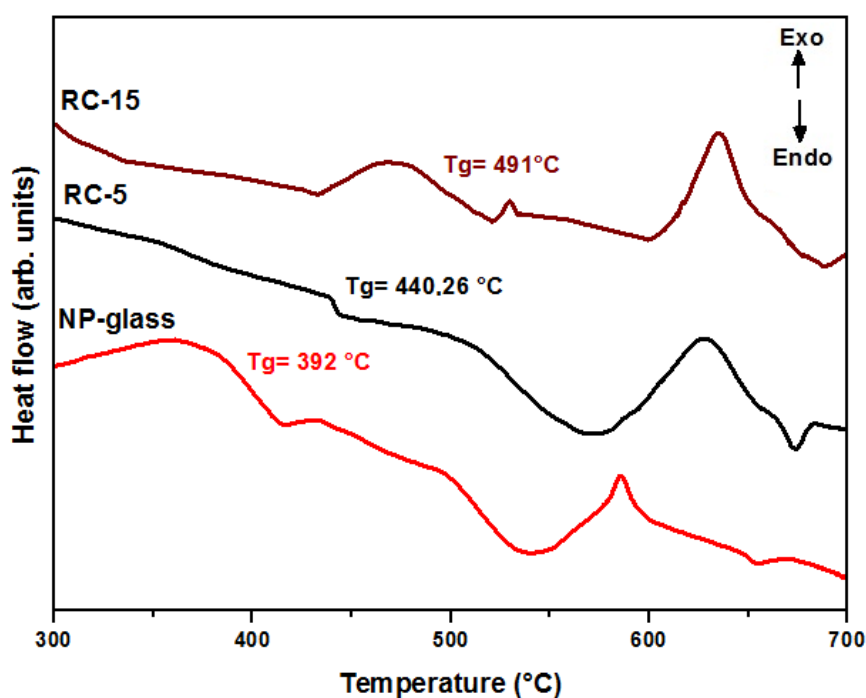

Figure 6. DSC curves for NP-glass, RC-5, and RC-15 phosphate glasses.

Table 6. Values of density (ρ_g), molar volume (Vm), and transition temperature (Tg) of the PGs.

Glass code	ρ_g (g.cm^{-3})	Vm (cm^3.mol^{-1})	Tg (°C)
NP-glass	2.6359	44.54	392
RC-2	2.8019	42.30	426
RC-5	2.8517	41.45	440
RC-10	2.9302	39.11	487
RC-15	2.9542	38.73	491

3.2.5. Infrared and Raman spectroscopies

The structural modifications of the elaborated glasses according to the oxide content in the clay were studied by infrared and Raman spectroscopies. The FTIR and Raman spectra of the investigated PGs (NP-glass, RC-2, RC-2, RC-5, RC-10, and RC-15) are shown in Fig. 7a and Fig. 7b, respectively. The assignments of the infrared and Raman bands are listed in Table 7.

Table 7. Infrared and Raman assignments (cm^{-1}) of the elaborated PGs.

Glass code	ν_{as}(PO$_2$)		ν_s(PO$_2$)		ν_{as}(PO$_3$) and ν_s(PO$_3$)		ν_{as}(POP)		ν_s(POP)		δ(PO$_4^{3-}$)	
	IR	Raman	IR	Raman	IR	Raman	IR	Raman	IR	Raman	IR	Raman
NP-glass	1298	1298	1173	1181	1095	-	910	940	760	698	526	-
RC-2	1298	1285	1173	1175	1093	-	910	940	760	692	527	501
RC-5	1296	1284	-	1175	1091	-	910	-	758	692	527	508
RC-10	1289	1280	1169	1173	1089	-	914	-	756	690	533	513
RC-15	1286	1280	-	1171	1087	-	914	-	754	690	540	-

As shown in Fig. 7a, six bands of the IR spectra of the reference glass were observed at 1298, 1173, 1095, 910, 760, and 526 cm^{-1}. There is no significant change in infrared spectra for glasses containing 2 and 5% by weight of clay. These results may be due to the conservation of the structure, which is essentially based on ultraphosphate groups (Q^3) [26]. The bands observed around 1298 and 1173 cm^{-1} are attributed to the asymmetric stretching vibration mode ν_{as}(PO$_2$) and symmetric ν_s(PO$_2$) where the two oxygen atoms without bridging (O-P-O) easily connect to a phosphorus atom in the phosphate tetrahedron in the intermediate structural units (Q^2) [8,24,25]. The band at 1095 cm^{-1} is attributed to the asymmetric stretching of the groups ν_{as}(PO$_3$) characteristic of the structural units (Q^1) [24,25]. With the addition of clay from 10% to 15% by weight, we notice the widening of these bands and a shift to lower wavenumbers with a reduction in intensity; this decrease in intensity reflects an increase in the contents of modifier oxides and suggests a reduction in the number of non-bridging P-O bonds with a progressive increase in connectivity [2,25,29].

Furthermore, the overlap of these bands can also be attributed to the Si-O(Si), and Si-O(P) links [2,25]. Also, the bands observed around 910 and 760 cm^{-1} in the IR spectra of the phosphate glasses were attributed to the symmetric and asymmetric stretching of the P-O-P bridge bonds, respectively. These two bands are obtained in species (Q^2) [24,25]. However, this time, the bands increased to higher wavenumbers around 916 cm^{-1} and decreased to lower wavenumbers of around 756 cm^{-1} with decreasing intensity for RC-10 and RC-15 glasses. These changes can be explained by the increase in the covalency of the P-O-P bonds which are replaced by that of P-O-M with the formation of chain termination units (Q^1) as the O/P ratio increases [2,9,20,25,29]. At last, the bands around 526 cm^{-1} are assigned to the deformation bands of the groups P-O$^-$ (PO$_4^{3-}$), vibration band of (O-P-O) in phosphate dimers (Q^1) [24,25].

The Raman spectrum of the reference glass (NP-glass) (Fig. 7b) reveals two full bands at 1298 and 1181 cm^{-1} that are attributed to the asymmetric and symmetric vibrations of P-O-P (ν_{as}(PO$_2$) and ν_s(PO$_2$)) in the chains (Q^2) [8,30]. The band at 698 cm^{-1} is attributed to the symmetric vibration ν_s(POP) of bridging oxygen connecting two tetrahedra PO$_4$ (P-O-P) in phosphate chains (Q^2) [8,30]. The band observed around 501 cm^{-1} is related to the deformation vibration of (O-P-O) in the structural chains (Q^1) [30]. With the increase in clay content, we observe a decrease in the general bottom in the ranges of 1100-1300 cm^{-1} and 600-800 cm^{-1}. These changes can be attributed to the breakage of P-O-P

bonds and the depolymerization of phosphate chains with the formation of the P-O-M bonds. Accordingly, as the O/P ratio increases, structural units (Q^1) are also formed [27,30]. We notice the appearance of a new band that probably comes from the vibrations of the Si-O-Si bridge in the silicon-oxygen units (Q^2) (about 620 cm^{-1}) [2].

Summing up the results of the FTIR and Raman spectroscopies and the values of the O/P ratio, it can be concluded that the structure of these glasses contains a mixture of ultraphosphate and polyphosphate structural units whose concentrations depend on the composition of the glasses.
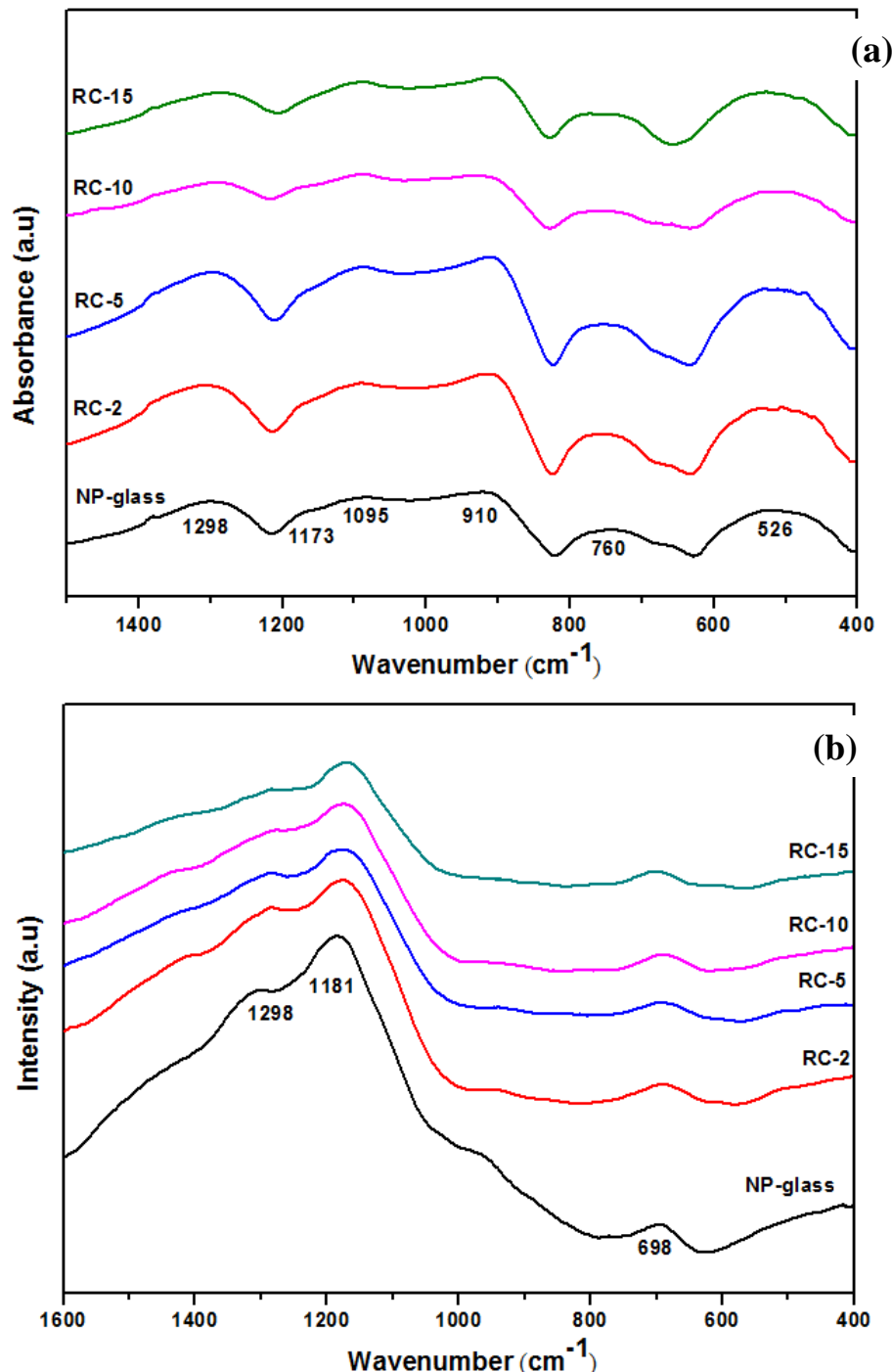

Figure 7. (a) FTIR spectra and (b) Raman spectra of the elaborated PGs with increasing RC content.

3.2.6. Chemical durability

In order **to show** the effect of oxides belonging to red clay on the chemical durability of glasses, the dissolution rate (D_R) as a function of the clay percentage at different pH values of the immersion solution is presented in Fig. 8. Clearly, for all

glasses, it is known that the dissolution rate is higher under basic conditions. However, for all pH values, the minimum D_R rate is observed for RC-15 glass which has the minimum molar percentage of P_2O_5. It should also be noted that, although density and Tg increase proportionally with the addition of clay,

chemical durability is also considerably improved. RC-15 glass also has a maximum value of these quantities. We can conclude that the chemical durability increases with increasing clay percentage up to 15% and that RC-15 glass is **the most resistant of these glasses**.
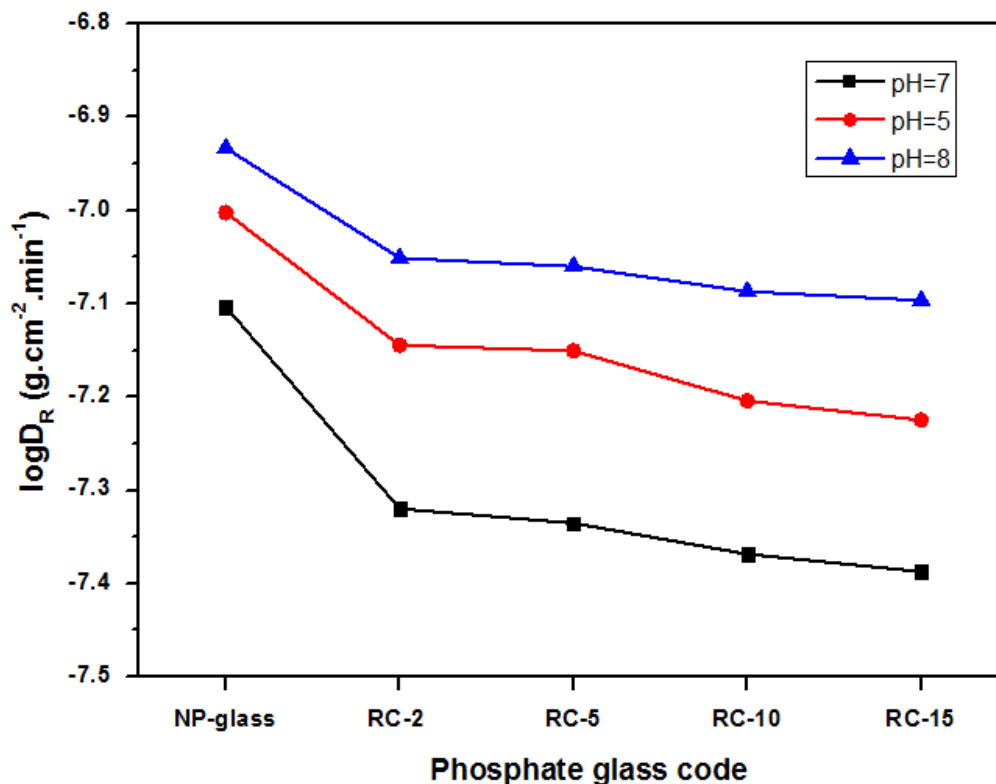

Figure 8. Variation of the dissolution rate D_R as a function of the weight percentage of red clay in PGs.

We can also affirm that the increase in the percentage of oxides such as SiO_2, Fe_2O_3, Al_2O_3, and MgO with the decrease in the percentage of oxides P_2O_5 and CaO in the structure of glass leads to the formation of P-O-Si, P-O-Fe, P-O-Al, and O-P-Mg bonds. Hence, this allows an increase in the bond strength, including the rigidity of the glass network, and leads to improved chemical durability of the glass.

Therefore, as compared to previous studies [31-37], it was confirmed that the dissolution of these phosphate glasses decreases with the increase of the added oxides belonging to the red clay.

4. Conclusions

In this paper, new phosphates glasses formulations based on Moroccan natural phosphate alone or with Moroccan red clay from the P_2O_5-SiO_2-CaO-Al_2O_3-MgO-Fe_2O_3-K_2O-Na_2O-TiO_2 complex system have been successfully prepared by the quenching method. Synthesized phosphate glasses containing mainly macroelements and microelements will be used to develop phosphate glass fibers acting as a slow-release fertilizer.

All elaborated phosphate glasses are homogeneous with a smooth surface, as shown by SEM analysis. The vitreous state of the elaborated glasses was confirmed by XRD and DSC. The structural changes investigated with FTIR and Raman spectroscopies suggested depolymerization and a stronger crosslinking of phosphate chains with the addition of the red clay increasing density and glass transition temperature. Conversely, the molar volume decreases monotonously with the introduction of clay. These changes were explained by the formation of the more covalent P-O-M bonds (with M= Si, Fe, Al, and Mg) replacing the P-O-P bonds, which also increases the rigidity of the glass network allowing the compactness of the structure.

The chemical durability of investigated phosphate glasses was evaluated in terms of dissolution rate (D_R), and the results show that the dissolution rate decreased with increasing of the red clay up to 15% by weight percentage for RC-15 glass belonging to the $41P_2O_5$-$23.5SiO_2$-$25CaO$-$3.9Al_2O_3$-$3.6MgO$-$2.9Fe_2O_3$-$3.2K_2O$-$0.6Na_2O$-$0.27TiO_2$ system. Based on the results, the chemical durability was improved with an increase in oxides belonging to the red clay.

References

1- M. Schumacher, L. Reither, J. Thomas, M. Kampschulte, U. Gbureck, A. Lode, and M. Gelinsky, Calcium phosphate bone cement/mesoporous bioactive glass composites for controlled growth factor delivery, Biomaterials Science, **2017**, 5(3), 578-588.

2- I. Waclawska, M. Szumera, and S. Justyna, Structural characterization of zinc-modified glasses from the SiO_2-P_2O_5-K_2O-CaO-MgO system, J. of Alloys and Compounds, **2016**, 666, 352-358.

3- N. Kitamura, A. Nomura, A. Saitoh, H. Kobayashi, I. Amamoto, and H. Takebe, Effect of ZrO_2 addition on water durability of FeO–Fe_2O_3–P_2O_5 glasses, J. of the Ceramic Society of Japan, **2018**, 126(11), 948-951.

4- L. Badr, Low-temperature conductivity and ion dynamics in silver iodide–silver metaphosphate glasses, Physical Chemistry Chemical Physics, **2017**, 19(32), 21527-21531.

5- H. Bih, L. Bih, B. Manoun, M. Azrour, B. Elouadi, and P. Lazor, Electrical Transport Properties of Iodine Oxide Phosphate Glasses Issued from The NaI-Li_2O-WO_3-P_2O_5 System, Moroccan Journal of Condensed Matter, **2010**, 12(2).

6- C. Chen, R. He, Y. Tan, B. Wang, S. Akhmadaliev, S. Zhou, S, and F. Chen, Optical ridge waveguides in Er^{3+}/Yb^{3+} co-doped phosphate glass produced by ion irradiation combined with femtosecond laser ablation for guided-wave green and red upconversion emissions, Optical Materials, **2016**, 51, 185-189.

7- M. Haouari, and N. Saad, On the Origin of the Large Stokes-Shift of the Emission of CdS Nanoparticles Embedded in a Phosphate Glass Matrix, J. of Cluster Science, **2018**, 29(2), 391-402.

8- A. Chahine, M. Et-Tabirou, M. Elbenaissi, M. Haddad, and J.L. Pascal, Effect of CuO on the structure and properties of (50−x/2) Na_2O−xCuO−(50− x/2) P_2O_5 glasses. Materials chemistry and physics, **2004**, 84(2-3), 341-347.

9- N. Sharmin, N., and C.D. Rudd, Structure, thermal properties, dissolution behaviour and biomedical applications of phosphate glasses and fibres: a review, Journal of Materials Science, **2017**, 52(15), 8733-8760.

10- G. K. Marasinghe, C.S. Ray, M. Karabulut, D. E Day, M. G. Shumsky, W.B. Yelon, and D.K. Shuh, Structural features of iron phosphate glasses, J. Non-Cryst Solids **1997**, 222, 144–52.

11- I. Ahmed, M. Lewis, I. Olsen, and J. C. Knowles, Phosphate glasses for tissue engineering: Part 1. Processing and characterisation of a ternary-based P_2O_5–CaO–Na_2O glass system, Biomaterials, **2004**, 25(3), 491-499.

12- H. Yung, P. Y. Shih, H. S. Liu, and T. S. Chin, Nitridation Effect on Properties of Stannous-Lead Phosphate Glasses, J. of the American Ceramic Society, **1997**, 80(9), 2213-2220.

13- R. A. Khan, A. J. Parsons, I. A. Jones, G. S. Walker, and C. D. Rudd, Degradation and interfacial properties of iron phosphate glass-fibre-reinforced PCL-based composite for synthetic bone replacement materials, Polymer-

Plastics Technology and Engineering, **2010**, 49(12), 1265-1274.

14- D. S. Brauer, C. Rüssel, and J. Kraft, Solubility of glasses in the system P_2O_5–CaO–MgO–Na_2O–TiO_2: Experimental and modeling using artificial neural networks, J. of non-crystalline solids, **2007**, 353(3), 263-270.

15- C. S. Ray, X. Fang, M. Karabulut, G.K. Marasinghe, D.E. Day, Effect of melting temperature and time on iron valence and crystallization of iron phosphate glasses, J. Non-Cryst Solids 1999, 249, 1–16.

16- M. Jerroudi, L. Bih, M. Azrour, B. Manoun, I. Saadoune, and P. Lazor, Investigation of Novel Low Melting Phosphate Glasses Inside the Na_2O–K_2O–ZnO–P_2O_5 System, J. of Inorganic and Organometallic Polymers and Materials, **2019**, 1-11.

17- G. Walter, J. Vogel, U. Hoppe, and P. Hartmann, The structure of CaO–Na_2O–MgO–P_2O_5 invert glass, J. of non-crystalline solids, **2001**, 296(3), 212-223.

18- F. Behrends, and H. Eckert, Mixed-Alkali Effects in Aluminophosphate Glasses: A Re-examination of the System [x Na_2O (1–x) Li_2O] 0.46 [y Al_2O_3 (1–y) P_2O_5] 0.54, The Journal of Physical Chemistry C, **2011**, 115(34), 17175-17183.

19- British Standards Institution, BS 10119, **2002**, London.

20- L. Abbas, L. Bih, A. Nadiri, Y. El Amraoui, H. Khemakhem, and D. Mezzane, Chemical durability of MoO_3-P_2O_5 and K_2O-MoO_3-P_2O_5 glasses, J. of Thermal Analysis and Calorimetry, **2007**, 90(2), 453-458.

21- M. Monsif, S. Rossignol, F. Allali, A. Zerouale, N. I. Kandri, E. Joussein, and R. Bertani, The implementation of geopolymers materials from Moroccan clay, within the framework of the valorization of the local natural resources, J. Mater. Environ. Sci, **2017**, 8, 2704-2721.

22- A. Qlihaa, S. Dhimni, F. Melrhaka, N. Hajjaji, and A. Srhiri, Physico-chemical characterization of a Morrocan clay, J. Mater. Environ. Sci, **2016**, 7(5), 1741-1750.

23- L. Ma, r. k. Brow, and M. E. Schlesinger, Dissolution behaviour of sodium-calcium polyphosphate glasses, Physics and Chemistry of Glasses-European Journal of Glass Science and Technology Part B, **2018**, 59(5), 205-212.

24- M. A. Cherbib, I. Khattech, L. Montagne, B. Revel, and M. Jemal, Structure properties relationship in calcium sodium metaphosphate and polyphosphate glasses, J. of Non-Crystalline Solids, **2018**, 485, 1-13.

25- W. Jastrzębski, M. Sitarz, M. Rokita, and K. Bułat, Infrared spectroscopy of different phosphates structures. Spectrochimica Acta Part A: Molecular and Biomolecular Spectroscopy, **2011**, 79(4), 722-727.

26- C. Tan, I. Ahmed, A. J. Parsons, N. Sharmin, C. Zhu, J. Liu, and X. Liu, Structural, thermal and dissolution properties of MgO-and CaO-

containing borophosphate glasses: effect of Fe_2O_3 addition, J. of materials science, **2017**, 52(12), 7489-7502.

27- R. O. Omrani, S. Krimi, J. J. Videau, I. Khattech, A. El Jazouli, and M. Jemal, Structural and thermochemical study of $Na_2O–ZnO–P_2O_5$ glasses, J. of Non-Crystalline Solids, **2014**, 390, 5-12.

28- N. H. Ray, Composition—property relationships in inorganic oxide glasses, J. of Non-Crystalline Solids, **1974**, 15(3), 423-434.

29- P. Rajbhandari, L. Montagne, and G. Tricot, Doping of low-Tg phosphate glass with Al_2O_3, B_2O_3 and SiO_2: Part II-insertion mechanism of Al_2O_3 and B_2O_3 in phosphate network characterized by 1D/2D solid-state NMR, Materials Chemistry and Physics, **2018**, 218, 122-129.

30- A. M. B. Silva, R. N. Correia, J. M. M. Oliveira, and M. H. V. Fernandes, Structural characterization of $TiO_2–P_2O_5–CaO$ glasses by spectroscopy, J. of the European Ceramic Society, **2010**, 30(6), 1253-1258.

31- M. S. Hasan, I. Ahmed, A. J. Parsons, G. S. Walker, and C. A. Scotchford, Material characterisation and cytocompatibility assessment of quinternary phosphate glasses, J. of Materials Science: Materials in Medicine, **2012**, 23(10), 2531-2541.

32- M. K. Hwang, and B. K. Ryu, Study on the water durability of zinc boro-phosphate glasses doped with MgO, Fe_2O_3, and TiO_2, J. of the Korean Physical Society, 2016, 69(2), 157-163.

33- A. Le Sauze, and R. Marchand, chemically durable nitrided phosphate glasses resulting from nitrogen/oxygen substitution within PO_4 tetrahedra, J. of Non-Crystalline Solids, **2000**, 263, 285-292.

34- I. Waclawska, and M. Szumera, Reactivity of silicate–phosphate glasses in the soil environment, J. of Alloys and Compounds, 2009, 468(1-2), 246-253.

35- H. K. Lee, S. J. Hwang, and W. H. Kang, Preparation of $K_2O-CaO-P_2O_5$ eco-glass fertilizers and effect in crops, In Materials Science Forum, Trans Tech Publications, **2005**, 486, 407-410.

36- H. Gao, T. Tan, and D. Wang, Dissolution mechanism and release kinetics of phosphate controlled release glasses in aqueous medium, J. of controlled release, **2004**, 96(1), 29-36.

37- K. Franks, V. Salih, J. C. Knowles, and I. Olsen, The effect of MgO on the solubility behavior and cell proliferation in a quaternary soluble phosphate based glass system, J. of Materials Science: Materials in Medicine, **2002**, 13(6), 549-556.

38- J. O. Byun, B. H. Kim, K. S. Hong, H. J. Jung, S. W. Lee, and A. A. Izyneev, Properties and structure of $RO–Na_2O–Al_2O_3–P_2O_5$ (R= Mg, Ca, Sr, Ba) glasses, J. of non-crystalline solids, **1995**, 190(3), 288-295.

39- U. B. Chanshetti, V. A. Shelke, S. M. Jadhav, S. G. Shankarwar, T. K. Chondhekar, A. G. Shankarwar, and M. S. Jogad, Density and molar volume studies of phosphate glasses, Facta universitatis-series: Physics, Chemistry and Technology, **2011**, 9(1), 29-36.